JACS Au
AN OPEN ACCESS JOURNAL OF THE AMERICAN CHEMICAL SOCIETY

pubs.acs.org/jacsau

Article

Sunlight-Driven Generation of Hypochlorous Acid on Plasmonic Au/AgCl Catalysts in Aerated Chloride Solution

Yasuhiro Shiraishi,* Yoshifumi Shimabukuro, Kaho Shima, Satoshi Ichikawa, Shunsuke Tanaka, and Takayuki Hirai

Cite This: *JACS Au* 2023, 3, 1403−1412

Read Online

ACCESS | Metrics & More | Article Recommendations | Supporting Information

ABSTRACT: HClO is typically manufactured from Cl_2 gas generated by the electrochemical oxidation of Cl^- using considerable electrical energy with a large concomitant emission of CO_2. Therefore, renewable energy-driven HClO generation is desirable. In this study, we developed a strategy for stable HClO generation by sunlight irradiation of a plasmonic Au/AgCl photocatalyst in an aerated Cl^- solution at ambient temperature. Plasmon-activated Au particles by visible light generate hot electrons, which are consumed by O_2 reduction, and hot holes, which oxidize the lattice Cl^- of AgCl adjacent to the Au particles. The formed Cl_2 is disproportionated to afford HClO, and the removed lattice Cl^- are compensated by the Cl^- in the solution, thus promoting a catalytic HClO generation cycle. A solar-to-HClO conversion efficiency of ∼0.03% was achieved by simulated sunlight irradiation, where the resultant solution contained >38 ppm (>0.73 mM) of HClO and exhibited bactericidal and bleaching activities. The strategy based on the Cl^- oxidation/compensation cycles will pave the way for sunlight-driven clean, sustainable HClO generation.

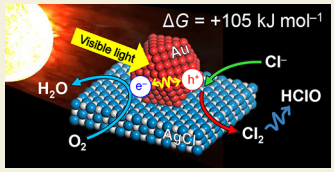

KEYWORDS: *photocatalysis, silver chloride, au particles, hypochlorous acid, solar-to-chemical conversion*

INTRODUCTION

Hypochlorous acid (HClO) is a strong, water-soluble oxidant that is widely used for disinfection, cleaning, deodorization, bleaching, and sterilization.[1−3] HClO is industrially produced from Cl_2 gas manufactured by chlor-alkali electrolysis in Cl^- solutions,[4−8] which involves the oxidation of Cl^- at the anode (eq 1) and the reduction of H^+ (eq 2) or O_2 (eq 3) at the cathode. The total reaction can be expressed as eq 4 or 5 (see Calculation of Gibbs free energy in Supporting Information). Dissolution of Cl_2 in water generates HClO by disproportionation according to the thermodynamic equilibrium (eq 6).[9] In contrast, deprotonation of HClO in basic media (eq 7) produces a hypochlorite anion (ClO^-), which has a lower oxidation ability than that of HClO.[10] The total electrolysis of the chlor-alkali processes (eq 4 or 5) is a thermodynamically up-hill reaction with a large Gibbs free energy gain and requires enormous electrical energy. Seventy million tons of HClO and related salts are annually produced in the world.[11] The total CO_2 emission resulting from the processing is estimated at 29 million tons.[12] Devising a clean, sustainable method for HClO production with renewable energy is necessary.

$$2Cl^- \rightarrow Cl_2 + 2e^- \ (+1.36\ \text{V vs NHE, pH 0}) \quad (1)$$

$$2H^+ + 2e^- \rightarrow H_2 \ (+0\ \text{V vs NHE, pH 0}) \quad (2)$$

$$O_2 + 4H^+ + 4e^- \rightleftharpoons 2H_2O \ (+1.23\ \text{V vs NHE, pH 0}) \quad (3)$$

$$2Cl^- + 2H^+ \rightarrow Cl_2 + H_2 \ (\Delta G^\circ = +342\ \text{kJ mol}^{-1}\ \text{at pH 7.0}) \quad (4)$$

$$2Cl^- + 1/2O_2 + 2H^+ \rightarrow Cl_2 + H_2O \ (\Delta G^\circ = +105\ \text{kJ mol}^{-1}\ \text{at pH 7.0}) \quad (5)$$

$$Cl_2 + H_2O \rightleftharpoons HClO + H^+ + Cl^- \ (K_1 = 3.94 \times 10^{-4}\ \text{M}^2\ \text{at 298 K}) \quad (6)$$

$$HClO \rightleftharpoons ClO^- + H^+ \ (K_2 = 2.62 \times 10^{-8}\ \text{M at 298 K}) \quad (7)$$

Sunlight is a promising renewable energy. Theoretically, semiconductor photocatalysis can generate HClO in Cl^- solutions under O_2 at ambient temperature (eq 5).[12] Photogenerated valence band (VB) holes (h_{VB}^+) oxidize Cl^- to generate Cl_2 (eq 1), which is readily transformed to HClO

Received: February 9, 2023
Revised: March 28, 2023
Accepted: April 21, 2023
Published: May 2, 2023

https://doi.org/10.1021/jacsau.3c00066
JACS Au 2023, 3, 1403−1412

Scheme 1. Electronic Band Structures of (a) Au and AgCl and (b) Au/AgCl[a]

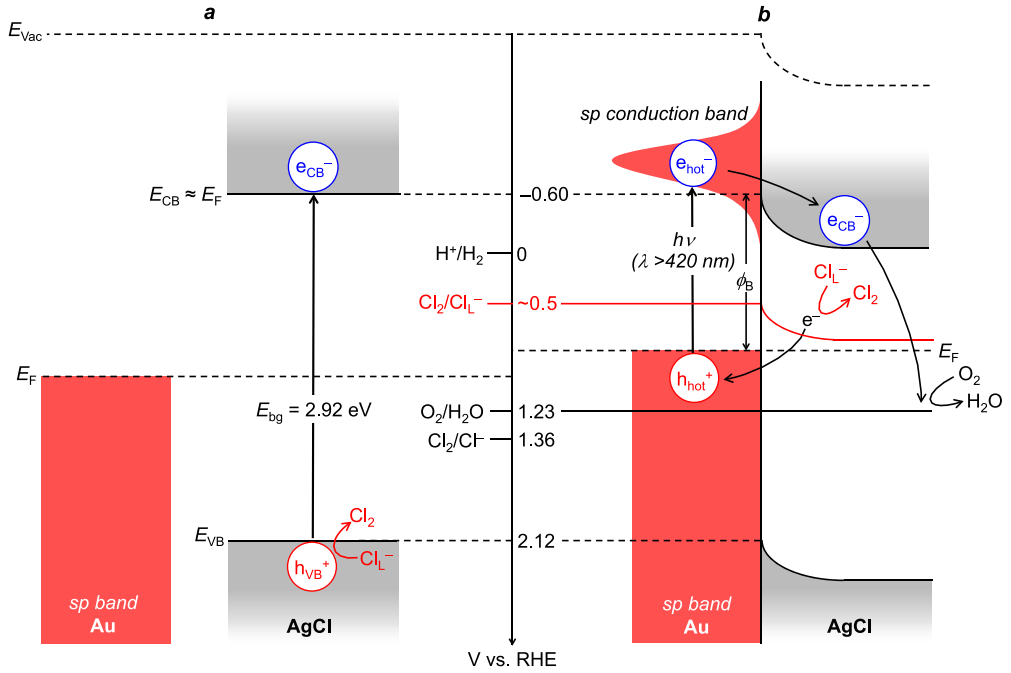

[a] E_F, E_{VB}, E_{CB}, E_{bg}, E_{vac}, and ϕ_B denote the Fermi level, valence band level, conduction band level, bandgap, vacuum level, and Schottky barrier height, respectively.

via disproportionation (eq 6), and simultaneously, the conduction band (CB) electrons (e_{CB}^-) reduce O_2 (eq 3). Some powder photocatalysts such as Pt-loaded TiO_2[13,14] and Pt-[15] or Pt-MnO_x-loaded WO_3[16] promote the reaction but produce solutions with low HClO concentrations (<2.4 ppm). This is because (i) oxidation of bulk Cl^- by h_{VB}^+ is difficult to promote owing to its deep potential level (eq 1); (ii) oxidation of bulk Cl^- is suppressed because oxidation of water by h_{VB}^+ (the reverse reaction of eq 3) occurs competitively; and (iii) these catalysts are mainly photoexcited by UV light (λ < 400 nm), which readily promotes the photodecomposition of HClO into O_2 and Cl^- (eq 8).[17,18] Therefore, the design of a photocatalyst that efficiently promotes Cl^- oxidation under visible light is necessary.

$$HClO \xrightarrow{h\nu\ (\lambda<400\ nm)} 1/2O_2 + H^+ + Cl^- \quad (8)$$

We selected AgCl powder, which is a nontoxic, inexpensive n-type semiconductor.[19] As shown in Scheme 1a, AgCl has a wide bandgap (~2.9 eV) and requires UV light for photoexcitation. Its density of states near the VB maximum consists of strongly hybridized Ag 4d and Cl 3p orbitals owing to the low electronegativity of Cl.[20] Therefore, a bandgap photoexcitation of AgCl promotes self-oxidation of the lattice Cl^- of AgCl (Cl_L^-) by the photogenerated h_{VB}^+, which has been observed for similar Cl^--containing semiconductors such as bismuth oxychlorides.[21] A notable feature of such Cl^--containing semiconductors is that the potential of self Cl_L^- oxidation lies at a more negative level [~0.5 V vs reversible hydrogen electrode (RHE), eq 9] than that of bulk Cl^- oxidation (1.36 V vs NHE, eq 1).[22] This implies that the self Cl_L^- oxidation of AgCl, if promoted in Cl^- solution under visible light, would generate HClO via the disproportionation of the formed Cl_2 (eq 6), and the removed Cl_L^- would be compensated from the Cl^- solution (eq 10), thereby promoting a stable catalytic HClO generation.

$$2AgCl_L \rightarrow Cl_2 + 2Ag^+ + 2e^- \ (\sim 0.5\ V\ vs\ RHE) \quad (9)$$

$$2Ag^+ + 2Cl^- \rightarrow 2AgCl_L \quad (10)$$

Localized surface plasmon resonance (LSPR) is a resonant oscillation of surface electrons of metal particles such as Au caused by incident photons of broader wavelength light.[23,24] This phenomenon has attracted considerable attention for solar-to-chemical conversion. Visible-light absorption of Au particles loaded on a semiconductor causes the collective oscillation of their sp-band electrons and generate hot hole (h_{hot}^+) and hot electron (e_{hot}^-) pairs and promote several oxidation and reduction reactions.[25−27] Notably, the potential of h_{hot}^+ lies at ~1.3 V (vs NHE),[28] which is more positive than the potential of Cl_L^- oxidation (~0.5 V). Therefore, we hypothesized that if Au particles are loaded onto AgCl particles (Scheme 1b), the h_{hot}^+ generated on the LSPR-activated Au particles would promote self Cl_L^- oxidation and facilitate visible-light-driven HClO generation. Therefore, in this study, we loaded Au particles onto the surface of AgCl powder (Au/AgCl) and used them for photocatalytic HClO generation in Cl^- solutions under aerated condition.

RESULTS AND DISCUSSION

Preparation and Characterization of Catalysts

AgCl powder was prepared by a precipitation method using $AgNO_3$ and KCl in water.[29] Au_x/AgCl catalysts [x (wt %) = Au/AgCl × 100] were prepared by the deposition−precipitation method.[30] AgCl was stirred in water containing $HAuCl_4 \cdot 4H_2O$, and the resultant was calcined in air at 673 K.[31] The Au loading amounts (x wt%) on the catalysts were determined by energy-dispersive X-ray fluorescence (XRF) analysis. Scanning electron microscopy (SEM) observations of AgCl and $Au_{2.7}$/AgCl (Figure S1) showed similar spherical AgCl particles with diameters of ~100 nm,[29] indicating that

https://doi.org/10.1021/jacsau.3c00066
JACS Au 2023, 3, 1403−1412

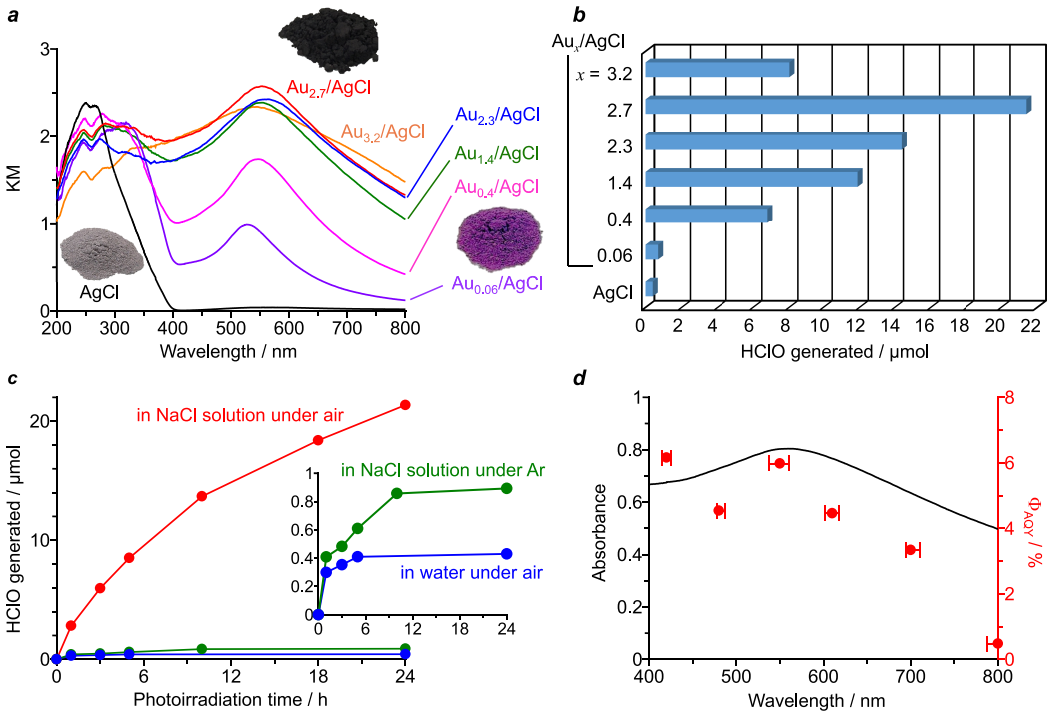

Figure 1. Optical and photocatalytic properties of catalysts. (a) Diffuse-reflectance UV−vis spectra. (b) Amount of HClO generated on the respective catalysts during photoirradiation. Conditions: 550 mM NaCl solution (50 mL), catalyst (0.1 g), air flow (1.0 L min^{-1}), λ > 420 nm (Xe lamp), photoirradiation time (24 h), and temperature (303 K). (c) Time course for the amount of HClO generated during photoreaction on $Au_{2.7}$/AgCl; inset: enlarged view. (d) Absorption spectrum of $Au_{2.7}$/AgCl and action spectrum for HClO generation on the catalyst.

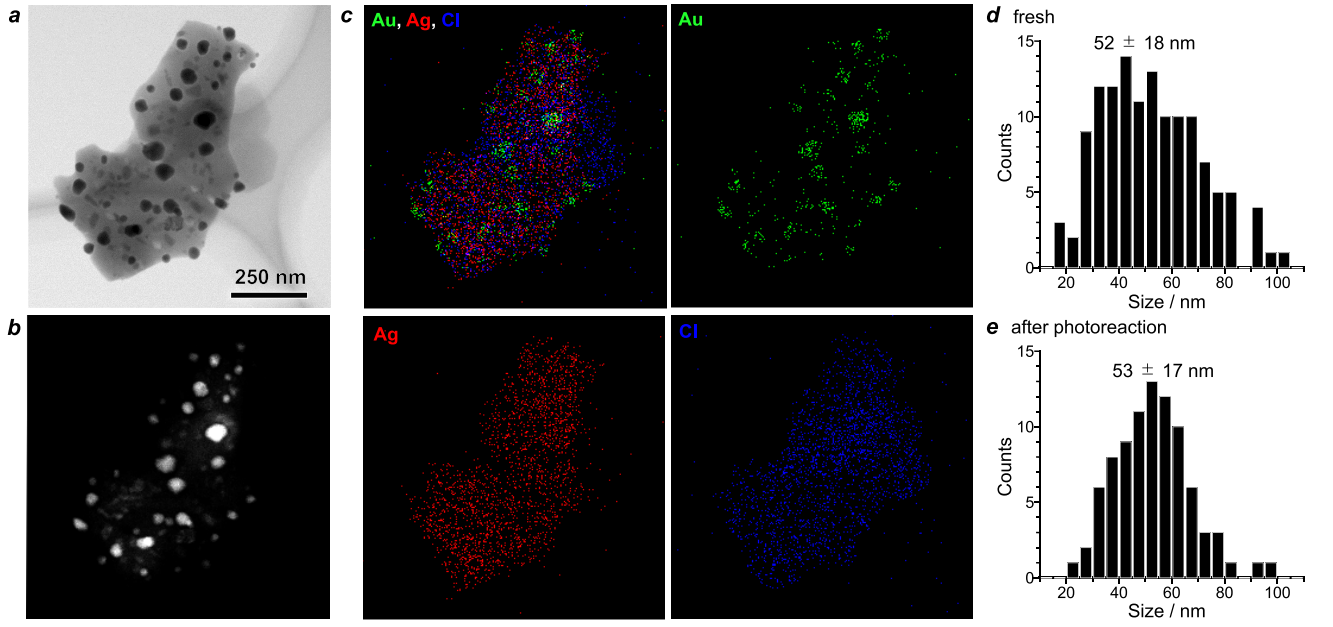

Figure 2. STEM-EDS observation results. (a) BF- and (b) ADF-STEM images of an $Au_{2.7}$/AgCl particle, and (c) its EDS maps (Lα1 line) of Au (green), Ag (red), and Cl (blue) components. Size distribution of Au particles on (d) fresh $Au_{2.7}$/AgCl and (e) the catalyst recovered after the photoreaction in NaCl solution under air flow for 24 h (Figure 1c, red).

the size and morphology of AgCl did not change with Au loading. As shown in Figure 1a, the diffuse-reflectance (DR) UV−vis spectrum of bare AgCl exhibits almost no absorption in the visible region (λ > 400 nm). A Tauc plot of the spectrum (Figure S2) revealed that the bandgap energy of AgCl was 2.92 eV (425 nm), suggesting that it scarcely absorbed visible light. The electrochemical Mott−Schottky plot of AgCl (Figure S3) revealed its flat-band potential as −0.60 V (vs RHE), which afforded the band structure of AgCl (Scheme 1a). In contrast, Au_x/AgCl exhibited a strong LSPR band of Au particles centered at 550 nm (Figure 1a)[32] and the absorbance increased with increasing Au loading (x).

X-ray diffraction (XRD) patterns of both AgCl and Au_x/AgCl (Figure S4) exhibited peaks assigned to cubic AgCl (JCPDS 31-1238), suggesting that its structure was maintained even after the Au loading. Au_x/AgCl also showed a diffraction

https://doi.org/10.1021/jacsau.3c00066
JACS Au 2023, 3, 1403−1412

Table 1. Surface Elemental Composition of Catalysts

			composition (mol %)[b]			Ag species (%)[c]		Au species (%)[d]	
entry	catalyst	status[a]	Ag	Cl	Au	Ag^0	Ag^+	Au^0	Au^{3+}
1	AgCl	fresh	50.0	50.0		3.5	96.5		
2	$Au_{2.7}$/AgCl	fresh	47.2	48.8	4.0	3.4	96.6	81.3	18.7
3	$Au_{2.7}$/AgCl	after photoirradiation in water under air	48.7	47.2	4.0	4.2	95.8	83.5	16.5
4	$Au_{2.7}$/AgCl	after photoirradiation in NaCl solution under air	47.1	48.9	4.0	3.3	96.7	83.6	16.4
5	$Au_{2.7}$/AgCl	after photoirradiation in NaCl solution under Ar	48.1	49.9	1.9	3.5	96.5	84.6	15.4

[a]Photoreactions were performed under conditions identical to those shown in Figure 1c (3 h). [b]Determined from the XPS peak areas with atomic sensitivity factors (Ag 3d, 34.06; Cl 2p, 4.15; Au 4f, 44.03) (Figures S9–S11). [c]Determined from Ag 3d XPS peak areas (Figure S10). [d]Determined from Au 4f XPS peak areas (Figure S11).

Scheme 2. Proposed Mechanism for Photocatalysis on Au/AgCl under Visible-Light Irradiation in Cl^- Solutions (a → b → c → a) with O_2 and (a → d → e) without O_2

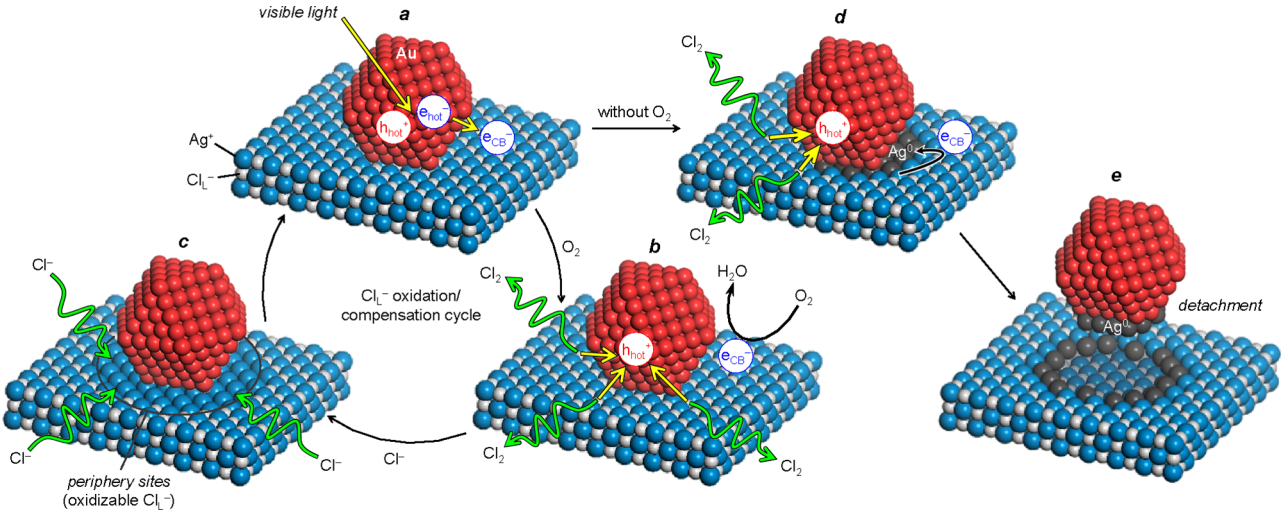

peak at 38°, which is attributed to the (111) facet of metallic Au (JCPDS 04-0784), indicating the formation of Au^0. Figure 2a and b show bright-field (BF) and annular dark-field (ADF) scanning transmission electron microscopy (STEM) images of $Au_{2.7}$/AgCl, respectively. Energy-dispersive X-ray spectroscopy (EDS)[33,34] elemental maps for Au, Ag, and Cl (Figure 2c) indicated that spherical or semi-spherical Au particles were homogeneously loaded on the AgCl surface. Other $Au_{2.7}$/AgCl particles exhibited similar STEM-EDS results (Figures S5–S7). The size distribution of the Au particles determined by the BF-STEM observations (Figure 2d) indicated that monodispersed Au particles with an average diameter of ∼50 nm were loaded on $Au_{2.7}$/AgCl.

X-ray photoelectron spectroscopy (XPS) was used to clarify the electronic states of Au, Ag, and Cl (Figure S8). The Ag 3d spectrum of bare AgCl (Figure S9) showed $3d_{5/2}$ and $3d_{3/2}$ peaks corresponding to the lattice Ag^+ (367.6, 373.6 eV) with a minor Ag^0 component.[35] In contrast, $Au_{2.7}$/AgCl showed these peaks at higher binding energies, suggesting that Au loading causes the transfer of the CB electrons of AgCl to Au particles to balance their Fermi levels,[36] thereby creating a Schottky barrier (ϕ_B) at the Au/AgCl interface (Scheme 1b). The Cl 2p spectra of both AgCl and $Au_{2.7}$/AgCl (Figure S10) showed $2p_{1/2}$ and $2p_{3/2}$ peaks for Cl_L^- (198.0, 199.6 eV)[37] at identical positions. The CB of AgCl mainly consists of Ag 5s states[20] and does not experience a shift of the Cl component after Au loading. The Au 4f spectrum of $Au_{2.7}$/AgCl (Figure S11) exhibited two components ascribed to Au^0 (84.7, 88.4 eV) and a small amount of Au^{3+} (86.9, 90.6 eV).[38] Surface elemental compositions of the catalysts were determined from the XPS peak areas using atomic sensitivity factors[39] (Table 1). The nearly 1:1 Ag:Cl composition of $Au_{2.7}$/AgCl (entry 2) agrees with the theoretical stoichiometry of AgCl (entry 1), indicating that the AgCl composition did not change after Au loading.

Photocatalysis

The photocatalytic activity of Au_x/AgCl was tested in NaCl solution. The Cl^- concentration in the solutions was set to 550 mM, which is the same as that in seawater.[18,21] A NaCl solution (50 mL) containing the catalyst (0.1 g) was irradiated by visible light (λ >420 nm) from a Xe lamp under air flow (1.0 L min^{-1}) and magnetic stirring at 303 K. Figure 1b shows the amount of HClO generated on the respective catalysts during 24 h of photoirradiation. Bare AgCl scarcely generated HClO. In contrast, Au_x/AgCl generated a larger amount of HClO, implying that the LSPR absorption of Au particles triggered HClO generation. Increasing the amount of Au loading enhanced the HClO generation, where $Au_{2.7}$/AgCl exhibited the highest activity. However, when Au particles were loaded onto other inorganic/organic semiconductor powders (TiO_2, WO_3, Fe_2O_3, Nb_2O_5, and g-C_3N_4) in a manner similar to that of $Au_{2.7}$/AgCl, negligible activities were observed (Figure S12) even though all of these catalysts exhibited LSPR bands of Au particles (Figure S13). This indicates that the Au/AgCl catalysts specifically show high activity for HClO generation.

The HClO generation on Au/AgCl is elucidated in Scheme 2, where (a) LSPR-activated Au particles generate h_{hot}^+ and

https://doi.org/10.1021/jacsau.3c00066
JACS Au 2023, 3, 1403–1412

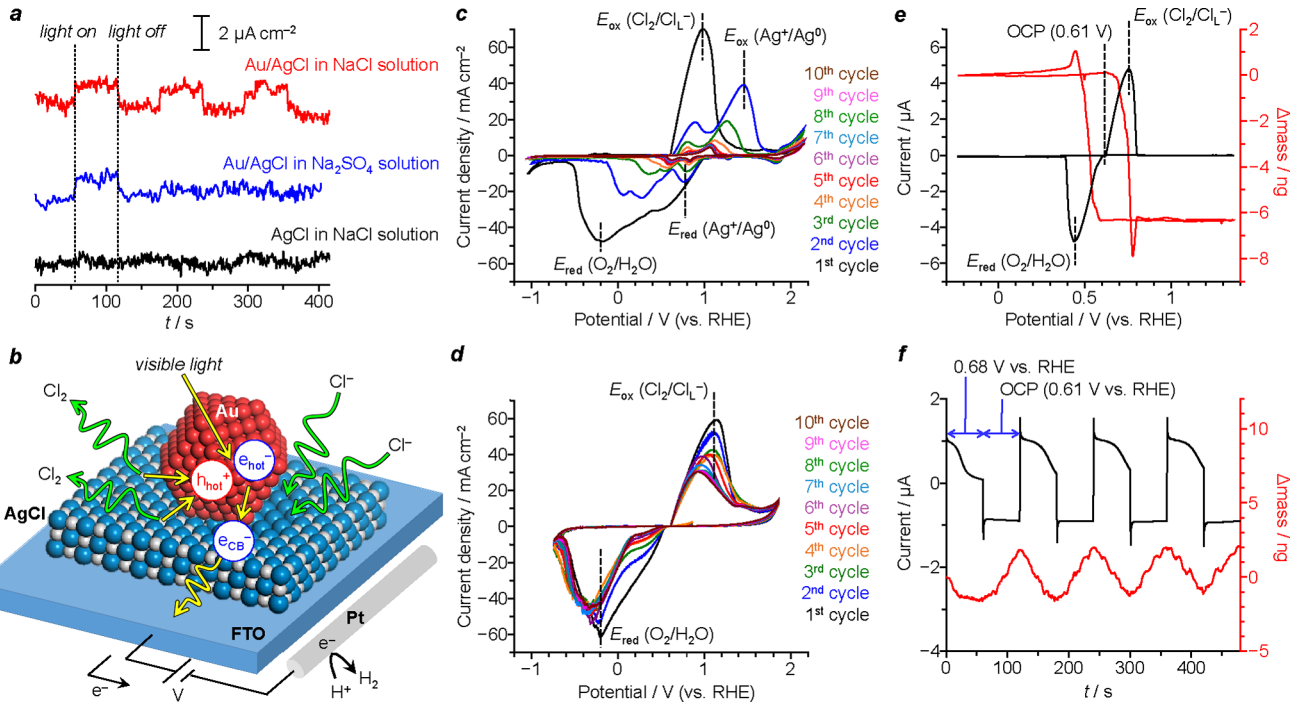

Figure 3. Electrochemical properties of the catalysts. (a) Photocurrent response of catalyst-loaded FTO in different electrolytes under Ar with $\lambda >$ 550 nm light irradiation at a bias of 1.0 V (vs Ag/AgCl). (b) Proposed mechanism for photocurrent generation on Au/AgCl-loaded FTO in Cl^- solution. CV of $Au_{2.7}$/AgCl-loaded FTO measured in (c) 100 mM Na_2SO_4 under O_2 and (d) 550 mM NaCl under O_2 (scan rate, 100 mV s^{-1}). (e) CV-QCM of $Au_{2.7}$/AgCl-loaded Au-QCM electrode measured in 550 mM NaCl under O_2 (scan rate, 2 mV s^{-1}), where a peak for O_2 reduction appears at a relatively positive potential because slow scan leads to consumption of O_2 in the system. (f) CA-QCM of $Au_{2.7}$/AgCl-loaded Au-QCM electrode measured in 550 mM NaCl under O_2. The potential at 0.68 V (vs RHE) and the OCP (0.61 V vs RHE) have been indicated in blue.

e_{hot}^- pairs and the injection of e_{hot}^- to the CB of AgCl generates e_{CB}^- (Scheme 1b); (b) h_{hot}^+ oxidizes Cl_L^- of AgCl in the periphery of Au particles to generate Cl_2, which is readily disproportionated to afford HClO (eq 6), while e_{CB}^- reduces O_2 (eq 3); and (c) the removed Cl_L^- is compensated from the solution. This Cl_L^- oxidation/compensation cycle catalytically generates HClO. Figure 1c presents the time profiles of the amount of HClO generated on $Au_{2.7}$/AgCl during visible-light irradiation under different conditions. Photoirradiation in pure water under air flow (blue) generated a small amount of HClO in the early stage (see inset), which was saturated at 0.4 μmol. The HClO generation in pure water indicates that the Cl_L^- of AgCl is oxidized by the LSPR activation of Au particles by visible light (Scheme 2b). The Cl_L^- oxidation was confirmed by XPS analysis (Table 1), where the Cl composition of $Au_{2.7}$/AgCl (48.8%, entry 2) decreased to 47.2% after the photoreaction in water (entry 3). In contrast, photoirradiation in a Cl^- solution (Figure 1c, red) stably generated HClO. In this case, the Cl content of the catalyst scarcely decreased (Table 1, entry 4). This suggests that, as shown in Scheme 2c, the eliminated Cl_L^- were successfully compensated by Cl^- in the solution, promoting catalytic HClO generation.

Notably, the catalyst maintained its high activity even after recycling it three times for the photoreaction in Cl^- solution under air (Figure S12). The SEM image (Figure S1) and XRD pattern (Figure S4) of the recovered catalyst were similar to those of the fresh catalyst. In addition, STEM-EDS observations of the recovered catalyst (Figures S14–S16) showed homogeneously distributed Au particles similar to those of the fresh catalyst (Figure 2, Figures S5–S7). Furthermore, the size distribution of the Au particles remains almost unchanged after the reaction (Figure 2e). These findings suggest that visible-light irradiation of Au/AgCl in an aerated Cl^- solution stably generates HClO without any activity and structural changes.

Mechanism for HClO Generation

The proposed catalytic cycle for HClO generation (Scheme 2ab → c) was confirmed through several analyses. Figure 1d shows the action spectrum for HClO generation on $Au_{2.7}$/AgCl under monochromated light irradiation. The highest apparent quantum yield (Φ_{AQY}) was obtained under 550 nm light irradiation, which is in good agreement with the LSPR band maximum of the Au particles. The generation of h_{hot}^+ and e_{hot}^- on Au particles followed by e_{hot}^- injection to AgCl (Scheme 2a) and consumption of h_{hot}^+ by Cl_L^- oxidation (Scheme 2b) were confirmed by the photocurrent response of catalyst-loaded fluorine tin oxide (FTO) electrodes (Figure 3a). Visible-light irradiation of bare AgCl in a NaCl solution (black) did not show any current, whereas $Au_{2.7}$/AgCl in a Na_2SO_4 solution (blue) generated a photocurrent. This indicates that e_{hot}^- generated on Au particles is transferred to the CB of AgCl and then to FTO, while h_{hot}^+ is consumed by the oxidation of Cl_L^- in the periphery of the Au particles (Figure 3b). However, in the case of $Au_{2.7}$/AgCl in a Na_2SO_4 solution (blue), the current density decreased during repeated light irradiation because the loss of Cl_L^- around the Au particles inhibited the consumption of h_{hot}^+. In contrast, $Au_{2.7}$/AgCl in a Cl^- solution (red) stably generated a current, indicating that the consumed Cl_L^- were compensated from a solution (Scheme 2c).

Cyclic voltammetry (CV) was performed using catalyst-loaded FTO electrodes to confirm the Cl_L^- oxidation/compensation cycle. Figure 3c shows the CV of $Au_{2.7}$/AgCl

https://doi.org/10.1021/jacsau.3c00066
JACS Au 2023, 3, 1403–1412

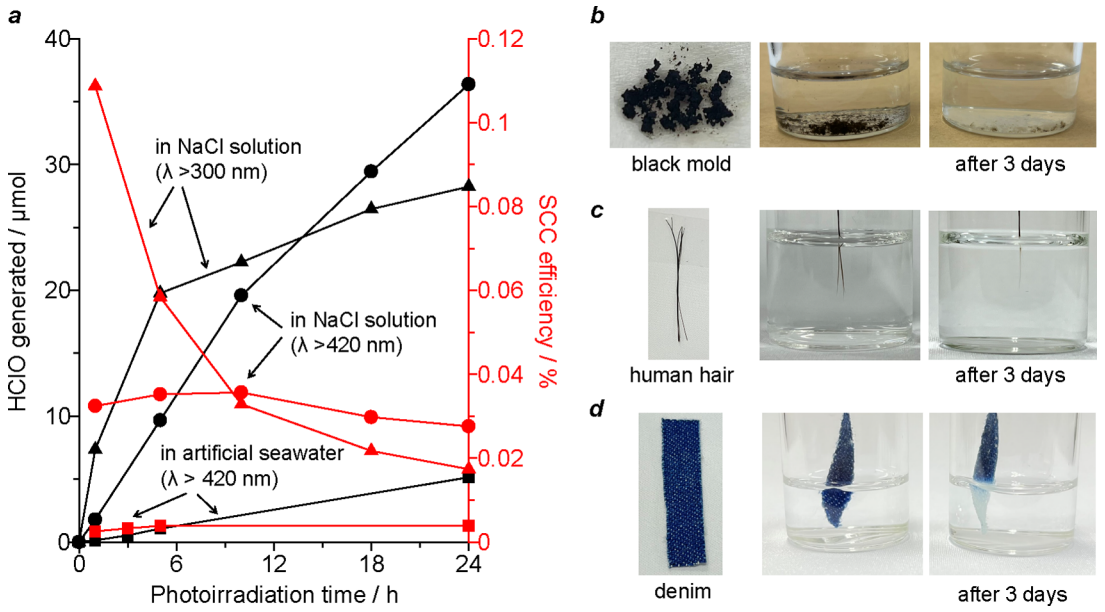

Figure 4. Solar-to-HClO conversion performance and oxidation capability of the obtained HClO solution. (a) Change in the amount of HClO generated and the SCC efficiency during photoreaction under simulated AM 1.5G sunlight (1 sun) irradiation. Conditions: NaCl solution or artificial seawater containing 550 mM Cl^- (50 mL), catalyst (0.1 g), air flow (1.0 L min^{-1}), and temperature (303 K). Photographs of (b) a black mold taken in a bathroom, (c) a human hair, and (d) a piece of denim pants, before and after 3 days in the HClO solution (38 ppm HClO) obtained after 24 h of photoirradiation (black circle in Figure 4a).

measured in Na_2SO_4 solution under O_2. The first cycle showed an anodic current for Cl_L^- oxidation at >0.6 V (vs RHE), indicating that the oxidation of Cl_L^- occurs at a more negative potential than that of the oxidation of bulk Cl^- (~1.5 V)[40] (Scheme 1b). A cathodic current for O_2 reduction appeared at <0 V, suggesting that e_{hot}^- is consumed by O_2 reduction (Scheme 1b). However, these currents disappeared after the second cycle, where reduction of Ag^+ (+0.8 V) and oxidation of the formed Ag^0 (+1.5 V) occurred irreversibly. In contrast, the CV of $Au_{2.7}$/AgCl in NaCl solution (Figure 3d) showed reversible anodic/cathodic currents for Cl_L^- oxidation/O_2 reduction. This confirms that the Au/AgCl catalyst in Cl^- solution stably promotes Cl_L^- oxidation/compensation (Scheme 2ab → c). Note that O_2 is reduced to water (eq 3). A rotating ring-disk electrode (RRDE) analysis with an $Au_{2.7}$/AgCl-loaded disc electrode confirms this. A linear-sweep voltammetry (LSV) analysis in an aerated solution (Figure S17) shows almost no ring current, where the H_2O_2 yield is less than 0.5% and the electron number for O_2 reduction is almost 4, indicating that O_2 is reduced to water (Scheme 2b).

Quartz crystal microbalance (QCM) analysis[41] was carried out to monitor the Cl_L^- oxidation/compensation on Au/AgCl. Figure 3e shows the results of CV-QCM analysis performed using the $Au_{2.7}$/AgCl-loaded QCM electrode in NaCl solution under O_2. The anodic current for Cl_L^- oxidation appeared at >0.6 V (vs RHE), which was accompanied by a decrease in the mass of the electrode; this is attributed to the removal of Cl_L^- by oxidation. However, a potential sweep to the negative side at <0.6 V recovered the mass of the electrode, which is indicative of Cl_L^- compensation from the solution. The Cl_L^- compensation was further confirmed by chronoamperometry (CA)-QCM analysis using $Au_{2.7}$/AgCl-loaded QCM electrodes in NaCl solution (Figure 3f). Applying a potential of +0.68 V (vs RHE) decreased the mass owing to the Cl_L^- oxidation, whereas applying no potential (open-circuit potential (OCP), +0.61 V) recovered the mass owing to the Cl_L^- compensation. The repeated mass decrease/recovery confirms the Cl_L^- oxidation/compensation cycle on Au/AgCl (Scheme 2a → b → c) and indicates that Cl_L^- compensation occurs quickly and quantitatively.

As shown in Scheme 2b,c, the h_{hot}^+ generated on the LSPR-activated Au particles oxidizes the Cl_L^- of AgCl in the periphery of the Au particles. As shown in Figure 1b, the catalyst with high Au loading (3.2 wt %) showed low HClO generation activity. $Au_{3.2}$/AgCl exhibited a broadened LSPR band (Figure 1a), suggesting the formation of larger-size Au particles by their coalescence during the thermal treatment.[31,32] This decreases the number of Cl_L^- adjacent to the Au particles that can be oxidized by h_{hot}^+, consequently decreasing photocatalytic activity. This finding confirms that the oxidation/compensation of the peripheral Cl_L^- promotes catalytic HClO generation. As shown in Figure 1c (blue), photoirradiation on $Au_{2.7}$/AgCl in pure water for 24 h generated 0.4 μmol HClO, suggesting that 0.8 μmol Cl_L^- is oxidized on the catalyst (eqs 1 and 6). In contrast, 21.4 μmol HClO was photogenerated in Cl^- solution for 24 h (Figure 1c, red), suggesting that 42.8 μmol Cl_L^- is oxidized. Therefore, the turnover number of the peripheral Cl_L^- is estimated to be ~54, indicating that the present system catalytically generates HClO by the Cl_L^- oxidation/compensation cycles (Scheme 2a → b → c).

Conditions for Efficient HClO Generation

A photoreaction under aerated conditions is essential for HClO generation: photoirradiation of $Au_{2.7}$/AgCl in Cl^- solution under Ar flow (Figure 1c, green) produced a small amount of HClO. The CV of $Au_{2.7}$/AgCl measured in a Cl^- solution under Ar (Figure S18) shows an irreversible current for Ag^+ reduction (+0.2 V), suggesting that the absence of O_2 promotes the reduction of Ag^+ in AgCl. XPS analysis of the recovered catalyst (Table 1, entry 5) revealed that the Au composition (4.0 mol %) decreased to 1.9 mol %. In addition,

https://doi.org/10.1021/jacsau.3c00066
JACS Au 2023, 3, 1403−1412

the Au LSPR band of the recovered catalyst decreased significantly (Figure S19), although the reaction under air scarcely changed the spectrum. This implies that, during photoreaction without O_2, e_{hot}^- is consumed by the reduction of Ag^+ in the periphery of the Au particles (Scheme 2d). The Ag^0 formed is adsorbed onto the Au particles and may weaken the Au−AgCl interaction, which can be involved in the removal of Au particles from the AgCl surface (Scheme 2a → d → e).

A Cl^- solution with a weakly acidic to neutral pH (4−7) is necessary. Figure S20 shows the total amount of Cl_2, HClO, and ClO^- in NaCl solutions after photoirradiation of $Au_{2.7}$/AgCl under different pH values. The reaction occurred efficiently at pH 4−7 but is suppressed at higher or lower pH, where the product amount profile agrees well with the mole fraction distribution of the HClO species determined based on eqs 6 and 7. At higher pH, a low H^+ concentration suppresses O_2 reduction (eq 3), thereby suppressing Cl_L^- oxidation. At lower pH, the disproportionation of the formed Cl_2 to HClO (eq 6) is suppressed, resulting in the removal of Cl_2 gas from the solution.

Ambient-temperature conditions are essential. As shown in Figure S21, higher reaction temperatures (313 and 333 K) decreased the activity owing to the thermal decomposition of the HClO formed,[42] indicating that a relatively low temperature (∼303 K) is favorable for HClO generation. Furthermore, a ∼500 mM Cl^- solution is appropriate. As shown in Figure S22, increasing the Cl^- concentration enhanced HClO generation on $Au_{2.7}$/AgCl, but the amount of HClO generated decreased when the Cl^- concentration was greater than 1 M. This activity decrease can be attributed to the increased solution viscosity, which affects the mass transfer during photocatalysis,[43] and to the decreased O_2 solubility,[44] which affects e_{hot}^- consumption. These results indicate that photoirradiation in aerated Cl^- solutions containing ∼500 mM Cl^- with weakly acidic−neutral pH (4−7) at ambient temperature is effective for HClO generation.

Solar Energy Conversion

The solar-to-chemical conversion (SCC) performance[45] of $Au_{2.7}$/AgCl was evaluated in aerated 550 mM NaCl solution under irradiation with AM1.5G simulated sunlight (1 sun) over the wavelength range of 300−2500 nm.[46,47] Figure 4a shows the change in the amount of HClO generated with photoirradiation time. Irradiating the entire wavelength of light (black triangle) efficiently generates HClO at the early stage of photoirradiation because direct photoexcitation of AgCl by UV light can promote Cl_L^- oxidation by h_{VB}^+ (Scheme 1a). However, the rate of HClO generation was nearly saturated at >6 h and the SCC efficiency decreased significantly with time. This is because the generated HClO absorbs UV light (Figure S23) and is subsequently decomposed into O_2 and Cl^- (eq 8).[17,18] As shown in Figure S24, irradiation with light at λ > 300 nm to a HClO solution generates a stoichiometric amount of O_2. However, irradiation with visible light (λ > 420 nm) scarcely decomposed HClO. As a result, as shown by the black circle in Figure 4a, irradiation with visible region light (λ > 420 nm) from the solar simulator to a Cl^- solution containing $Au_{2.7}$/AgCl suppressed subsequent decomposition of HClO and stably generated HClO. The SCC efficiency was estimated as ∼0.03% based on the formation of HClO and remained constant during the photoirradiation. Notably, the HClO concentration in this case was higher than that obtained under irradiation with light of the entire wavelength range (λ > 300 nm). The results indicate that visible-light irradiation stably promotes the up-hill reaction (eq 5) and facilitates solar-to-HClO conversion.

The irradiation of an NaCl solution with visible light (λ > 420 nm) for 24 h under air (black circle, Figure 4a) generated 38 ppm of HClO (36 μmol/50 mL). This concentration is higher than that obtained in the reported photocatalytic systems (<2.4 ppm)[12−16] or photoelectrochemical systems using photoanodes with external bias (<35 ppm),[48,49] confirming the high activity of the present Au/AgCl system. In addition, this concentration (38 ppm) is much higher than the HClO concentration (>3 ppm) recommended by WHO for the disinfection of drinking water,[50] where an HClO solution of >3 ppm has been confirmed to be effective for the disinfection of several types of bacteria and viruses in lakes, rivers, and groundwater containing fecal contamination.[1,51] This means that the HClO solution obtained in our experiment has sufficient bactericidal activity. The oxidation capability of the solution was confirmed by testing it in real-world scenarios. A black mold, which is *Cladosporium* spp., one of the most abundant airborne spores in the world,[52] was taken from a bathroom and left in the obtained HClO solution for 3 days (Figure 4b). The color was nearly bleached owing to the decomposition of the mold spores.[53] In addition, the obtained HClO solution successfully bleached the black melanin dye in human hair (Figure 4c) and the indigo dye in denim pants (Figure 4d). These results confirmed the oxidation capability of the obtained HClO solution for sterilization and bleaching.

Seawater is a naturally abundant Cl^- solution but ineffective for the present photoprocess. As shown in Figure 4a (denoted by square keys), the photoreaction in artificial seawater containing 550 mM Cl^-, which was prepared by dissolving red sea salt, generated a small amount of HClO and showed low SCC efficiency (∼0.004%). This is ascribed to the small amount of bicarbonate anions (HCO_3^-, ∼3 mM) present in seawater. Seawater contains several cations (Na^+, Li^+, K^+, Ca^{2+}, Mg^{2+}, Sr^{2+}, and Ba^{2+}) and anions (SO_4^{2-}, HCO_3^-, Br^-, and F^-) in different amounts (Table S1).[54] To clarify the effect of these coexisting ions on the HClO generation, photoreactions were performed on $Au_{2.7}$/AgCl in aerated 550 mM NaCl solution containing 50 mM of each of the respective cations and anions (Figure S25). All the cations and SO_4^{2-}, Br^-, and F^- anions scarcely affected HClO generation, but HCO_3^- significantly decreased the activity. The CV of $Au_{2.7}$/AgCl measured in NaCl solution with HCO_3^- (Figure S26) showed that the current density of Cl_L^- oxidation decreased during the cycles. This indicates that HCO_3^- in solution may compensate for the removed Cl_L^- of AgCl to form Ag_2CO_3;[55] this replacement may suppress Cl_L^- oxidation and decrease the activity for HClO generation. These findings indicate that the present photoprocess based on the Cl_L^- oxidation/compensation is affected by even a small amount of HCO_3^- impurity. Nevertheless, our strategy, which stably produces a high-HClO-content solution with a strong oxidation capability using an inexpensive Cl^- solution under irradiation of visible light, remains promising for clean and sustainable HClO generation.

CONCLUSIONS

We demonstrated that Au/AgCl plasmonic photocatalysts can generate HClO in aerated Cl^- solutions at ambient temperature under irradiation of visible light from sunlight. The LSPR-activated Au particles generate e_{hot}^- and h_{hot}^+. e_{hot}^- is

https://doi.org/10.1021/jacsau.3c00066
JACS Au 2023, 3, 1403−1412

consumed by the reduction of O_2, and h_{hot}^+ oxidizes Cl_L^- of AgCl in the periphery of the Au particles, where the formed Cl_2 is transformed to HClO via disproportionation. The removed Cl_L^- of AgCl is compensated by Cl^- in solution, thereby promoting catalytic HClO generation. The present system generates HClO solutions, which possess a high oxidation capability for sterilization and bleaching, although HCO_3^- impurities that deactivate the catalyst surface must be removed from the solution for efficient HClO generation. The powder photocatalyst system is a low-cost technology with the potential to enable scale-up to larger systems owing to simple catalyst preparation and simple reactor/facility designs. Therefore, HClO production by a powder photocatalyst system is not only economical but also contributes to mitigation of global warming. The HClO concentration obtained by the present system is much lower than that of commercially available HClO solution. Therefore, further activity enhancement is necessary for practical applications. Nevertheless, the Au/AgCl powder photocatalyst system presented here, based on the Cl_L^- oxidation/compensation by LSPR activation, may contribute to clean, sustainable production of HClO using renewable solar energy.

■ ASSOCIATED CONTENT

Supporting Information

The Supporting Information is available free of charge at https://pubs.acs.org/doi/10.1021/jacsau.3c00066.

Experimental procedure, calculation of Gibbs free energy, components in seawater (Table S1), SEM (Figure S1), Tauc plot (S2), Mott−Schottky plot (S3), XRD (S4), STEM-EDS of fresh catalysts (S5−S7), XPS (S8−S11), HClO generation on other Au catalysts (S12), DR UV−vis spectra of other Au catalysts (S13), STEM-EDS of the used catalyst (S14−S16), RRDE (S17), CV under Ar (S18), DR UV−vis spectra of the used catalyst (S19), effect of several parameters on HClO generation (S20−S22), absorption spectra of HClO and photodecomposition data (S23, S24), effect of ions on HClO generation (S25), CV with $NaHCO_3$ (S26), light emission spectra (S27), calibration curve for HClO (S28), and references (PDF)

■ AUTHOR INFORMATION

Corresponding Author

Yasuhiro Shiraishi − *Research Center for Solar Energy Chemistry and Division of Chemical Engineering, Graduate School of Engineering Science, Osaka University, Toyonaka 560-8531, Japan; Innovative Catalysis Science Division, Institute for Open and Transdisciplinary Research Initiatives (ICS-OTRI), Osaka University, Suita 565-0871, Japan;* orcid.org/0000-0003-1812-0644; Email: shiraishi.yasuhiro.es@osaka-u.ac.jp

Authors

Yoshifumi Shimabukuro − *Research Center for Solar Energy Chemistry and Division of Chemical Engineering, Graduate School of Engineering Science, Osaka University, Toyonaka 560-8531, Japan*

Kaho Shima − *Research Center for Solar Energy Chemistry and Division of Chemical Engineering, Graduate School of Engineering Science, Osaka University, Toyonaka 560-8531, Japan*

Satoshi Ichikawa − *Research Center for Ultra-High Voltage Electron Microscopy, Osaka University, Ibaraki 567-0047, Japan*

Shunsuke Tanaka − *Department of Chemical, Energy, and Environmental Engineering, Kansai University, Suita 564-8680, Japan;* orcid.org/0000-0001-5157-3317

Takayuki Hirai − *Research Center for Solar Energy Chemistry and Division of Chemical Engineering, Graduate School of Engineering Science, Osaka University, Toyonaka 560-8531, Japan*

Complete contact information is available at: https://pubs.acs.org/10.1021/jacsau.3c00066

Author Contributions

All authors equally contributed. CRediT: **Yasuhiro Shiraishi** conceptualization, data curation, formal analysis, funding acquisition, investigation, methodology, project administration, resources, supervision, validation, visualization, writing-review & editing; **Yoshifumi Shimabukuro** data curation, formal analysis, investigation, visualization, writing-original draft; **Kaho Shima** data curation, formal analysis, investigation, writing-original draft; **Satoshi Ichikawa** formal analysis, investigation; **Shunsuke Tanaka** formal analysis, investigation; **Takayuki Hirai** supervision, writing-review & editing.

Notes

The authors declare no competing financial interest.

■ ACKNOWLEDGMENTS

This work was supported by a Grant-in-Aid for Scientific Research (No. 21H01707) and Nanotechnology Platform Project (Nos. JPMXP09A20OS0033 and JPMXP09A21OS0006) from the Ministry of Education, Culture, Sports, Science and Technology, Japan (MEXT).

■ REFERENCES

(1) Rutala, W. A.; Weber, D. J. Uses of inorganic hypochlorite (bleach) in health-care facilities. *Clin. Microbiol. Rev.* **1997**, *10*, 597−610.

(2) Wang, L.; Bassiri, M.; Najafi, R.; Najafi, K.; Yang, J.; Khosrovi, B.; Hwong, W.; Barati, E.; Belisle, B.; Celeri, C.; Robson, M. C. Hypochlorous acid as a potential wound care agent: part I. Stabilized hypochlorous acid: a component of the inorganic armamentarium of innate immunity. *J. Burns Wounds* **2007**, *6*, 65−79.

(3) Mikutta, R.; Kleber, M.; Kaiser, K.; Jahn, R. Organic matter removal from soils using hydrogen peroxide, sodium hypochlorite, and disodium peroxodisulfate. *Soil Sci. Soc. Am. J.* **2005**, *69*, 120−135.

(4) Viswanathan, K.; Tilak, B. V. Chemical, electrochemical, and technological aspects of sodium chlorate manufacture. *J. Electrochem. Soc.* **1984**, *131*, 1551−1559.

(5) Karlsson, R. K. B.; Cornell, A. Selectivity between oxygen and chlorine evolution in the chlor-alkali and chlorate processes. *Chem. Rev.* **2016**, *116*, 2982−3028.

(6) Kraft, A.; Stadelmann, M.; Blaschke, M.; Kreysig, D.; Sandt, B.; Schröder, F.; Rennau, J. Electrochemical water disinfection. Part I: Hypochlorite production from very dilute chloride solutions. *J. Appl. Electrochem.* **1999**, *29*, 861−868.

(7) Czarnetzki, L. R.; Janssen, L. J. J. Formation of hypochlorite, chlorate and oxygen during NaCl electrolysis from alkaline solutions at an RuO_2/TiO_2 anode. *J. Appl. Electrochem.* **1992**, *22*, 315−324.

(8) Moussallem, I.; Jörissen, J.; Kunz, U.; Pinnow, S.; Turek, T. Chlor-alkali electrolysis with oxygen depolarized cathodes: History, present status and future prospects. *J. Appl. Electrochem.* **2008**, *38*, 1177−1194.

(9) Connick, R. E.; Chia, Y.-T. The hydrolysis of chlorine and its variation with temperature. *J. Am. Chem. Soc.* **1959**, *81*, 1280−1284.
(10) Czarnetzki, L. R. *Aspects of electrochemical production of hypochlorite and chlorate*, Technische Universiteit Eindhoven: Eindhoven, 1989.
(11) *Chemical Economics Handbook, Hypochlorite Bleaches*; IHS Markit, 2015.
(12) Sayama, K. Production of high-value-added chemicals on oxide semiconductor photoanodes under visible light for solar chemical-conversion processes. *ACS Energy Lett.* **2018**, *3*, 1093−1101.
(13) Huang, L.; Li, R.; Chong, R.; Liu, G.; Han, J.; Li, C. Cl^- making overall water splitting possible on TiO_2-based photocatalysts. *Catal. Sci. Technol.* **2014**, *4*, 2913−2918.
(14) Reichman, B.; Byvik, C. E. Photoproduction of I_2, Br_2, and Cl_2 on n-semiconducting powder. *J. Phys. Chem.* **1981**, *85*, 2255−2258.
(15) Pang, R.; Miseki, Y.; Okunaka, S.; Sayama, K. Photocatalytic production of hypochlorous acid over Pt/WO_3 under simulated solar light. *ACS Sustainable Chem. Eng.* **2020**, *8*, 8629−8637.
(16) Pang, R.; Miseki, Y.; Sayama, K. Enhanced HClO production from chloride by dual cocatalyst loaded WO_3 under visible light. *Catal. Sci. Technol.* **2022**, *12*, 2935−2942.
(17) Watts, M. J.; Linden, K. G. Chlorine photolysis and subsequent OH radical production during UV treatment of chlorinated water. *Water Res.* **2007**, *41*, 2871−2878.
(18) Mase, K.; Yoneda, M.; Yamada, Y.; Fukuzumi, S. Seawater usable for production and consumption of hydrogen peroxide as a solar fuel. *Nat. Commun.* **2016**, *7*, 11470.
(19) Tian, B.; Zhang, J. Morphology-controlled synthesis and applications of silver halide photocatalytic materials. *Catal. Surv. Asia* **2012**, *16*, 210−230.
(20) De Boer, P. K.; De Groot, R. A. Conduction band of the photographic compound AgCl. *J. Phys. Chem. A* **1999**, *103*, 5113−5115.
(21) Fujito, H.; Kunioku, H.; Kato, D.; Suzuki, H.; Higashi, M.; Kageyama, H.; Abe, R. Layered perovskite oxychloride Bi_4NbO_8Cl: A stable visible light responsive photocatalyst for water splitting. *J. Am. Chem. Soc.* **2016**, *138*, 2082−2085.
(22) Shiraishi, Y.; Hashimoto, M.; Chishiro, K.; Moriyama, K.; Tanaka, S.; Hirai, T. Photocatalytic dinitrogen fixation with water on bismuth oxychloride in chloride solutions for solar-to-chemical energy conversion. *J. Am. Chem. Soc.* **2020**, *142*, 7574−7583.
(23) Linic, S.; Christopher, P.; Ingram, D. B. Plasmonic-metal nanostructures for efficient conversion of solar to chemical energy. *Nat. Mater.* **2011**, *10*, 911−921.
(24) Brongersma, M. L.; Halas, N. J.; Nordlander, P. Plasmon-induced hot carrier science and technology. *Nat. Nanotechnol.* **2015**, *10*, 25−34.
(25) Zhang, Y.; He, S.; Guo, W.; Hu, Y.; Huang, J.; Mulcahy, J. R.; Wei, W. D. Surface-plasmon-driven hot electron photochemistry. *Chem. Rev.* **2018**, *118*, 2927−2954.
(26) Aslam, U.; Rao, V. G.; Chavez, S.; Linic, S. Catalytic conversion of solar to chemical energy on plasmonic metal nanostructures. *Nat. Catal.* **2018**, *1*, 656−665.
(27) Cortés, E.; Besteiro, L. V.; Alabastri, A.; Baldi, A.; Tagliabue, G.; Demetriadou, A.; Narang, P. Challenges in plasmonic catalysis. *ACS Nano* **2020**, *14*, 16202−16219.
(28) Tatsuma, T.; Nishi, H. Plasmonic hole ejection involved in plasmon-induced charge separation. *Nanoscale Horiz.* **2020**, *5*, 597−606.
(29) Liu, S.; Zhang, Q.; Li, H.; Yang, Y.; Tian, X.; Whiting, A. A visible-light-induced α-H chlorination of alkylarenes with inorganic chloride under Nano Ag@AgCl. *Chem. Eur. J.* **2015**, *21*, 9671−9675.
(30) Haruta, M. Size- and support-dependency in the catalysis of gold. *Catal. Today* **1997**, *36*, 153−166.
(31) Tsukamoto, D.; Shiraishi, Y.; Sugano, Y.; Ichikawa, S.; Tanaka, S.; Hirai, T. Gold nanoparticles located at the interface of anatase/rutile TiO_2 particles as active plasmonic photocatalysts for aerobic oxidation. *J. Am. Chem. Soc.* **2012**, *134*, 6309−6315.
(32) Shiraishi, Y.; Yasumoto, N.; Imai, J.; Sakamoto, H.; Tanaka, S.; Ichikawa, S.; Ohtani, B.; Hirai, T. Quantum tunneling injection of hot electrons in Au/TiO_2 plasmonic photocatalysts. *Nanoscale* **2017**, *9*, 8349−8361.
(33) Parish, M. C. Multivariate statistics applications in scanning transmission electron microscopy X-ray spectrum imaging. *Adv. Imaging Electron Phys.* **2011**, *168*, 249−295.
(34) Shiraishi, Y.; Matsumoto, M.; Ichikawa, S.; Tanaka, S.; Hirai, T. Polythiophene-doped resorcinol−formaldehyde resin photocatalysts for solar-to-hydrogen peroxide energy conversion. *J. Am. Chem. Soc.* **2021**, *143*, 12590−12599.
(35) Han, C.; Ge, L.; Chen, C.; Li, Y.; Zhao, Z.; Xiao, X.; Li, Z.; Zhang, J. Site-selected synthesis of novel Ag@AgCl nanoframes with efficient visible light induced photocatalytic activity. *J. Mater. Chem. A* **2014**, *2*, 12594−12600.
(36) Liu, S.; Chai, J.; Sun, S.; Zhang, L.; Yang, J.; Fu, X.; Hai, J.; Jing, Y. H.; Wang, B. Site-selective photosynthesis of Ag−AgCl@Au nanomushrooms for NIR-II light-driven O_2- and $O_2^{\bullet-}$-evolving synergistic photothermal therapy against deep hypoxic tumors. *ACS Appl. Mater. Interfaces* **2021**, *13*, 46451−46463.
(37) Xu, H.; Li, H.; Xia, J.; Yin, S.; Luo, Z.; Liu, L.; Xu, L. One-pot synthesis of visible-light-driven plasmonic photocatalyst Ag/AgCl in ionic liquid. *ACS Appl. Mater. Interfaces* **2011**, *3*, 22−29.
(38) Casaletto, M. P.; Longo, A.; Martorana, A.; Prestianni, A.; Venezia, A. M. XPS study of supported gold catalysts: the role of Au^0 and $Au^{+\delta}$ species as active sites. *Surf. Interface Anal.* **2006**, *38*, 215−218.
(39) Scofield, J. H. Hartree-Slater subshell photoionization cross-sections at 1254 and 1487 eV. *J. Electron Spectrosc. Relat. Phenom.* **1976**, *8*, 129−137.
(40) Fuku, K.; Sayama, K. Efficient oxidative hydrogen peroxide production and accumulation in photoelectrochemical water splitting using a tungsten trioxide/bismuth vanadate photoanode. *Chem. Commun.* **2016**, *52*, 5406−5409.
(41) Muratsugu, M.; Ohta, F.; Miya, Y.; Hosokawa, T.; Kurosawa, S.; Kamo, N.; Ikeda, H. Quartz crystal microbalance for the detection of microgram quantities of human serum albumin: relationship between the frequency change and the mass of protein adsorbed. *Anal. Chem.* **1993**, *65*, 2933−2937.
(42) Lister, M. W. Decomposition of sodium hypochlorite: The uncatalyzed reaction. *Can. J. Chem.* **1956**, *34*, 465−478.
(43) Lin, J.; Li, Y.; Xie, B. Heterogeneous photocatalytic performances of CO_2 reduction based on the $[Emim]BF_4$ + TEOA + H_2O system. *RSC Adv.* **2019**, *9*, 35841−35846.
(44) Janata, E.; Kelm, M.; Ershov, B. G. Solubility of oxygen and nitrous oxide in aqueous solutions of NaCl: A pulse radiolysis study. *Radiat. Phys. Chem.* **2002**, *63*, 157−160.
(45) Shiraishi, Y.; Takii, T.; Hagi, T.; Mori, S.; Kofuji, Y.; Kitagawa, Y.; Tanaka, S.; Ichikawa, S.; Hirai, T. Resorcinol−formaldehyde resins as metal-free semiconductor photocatalysts for solar-to-hydrogen peroxide energy conversion. *Nat. Mater.* **2019**, *18*, 985−993.
(46) Gordon, I.; Krebs, F. C.; Mathew, X.; Lampert, C. M.; Rougier, A.; Smestad, G. P.; Subrahmanyam, A. Editorial. *Sol. Energy Mater. Sol. Cells* **2015**, *133*, A1−A6.
(47) Shiraishi, Y.; Ueda, Y.; Soramoto, A.; Hinokuma, S.; Hirai, T. Photocatalytic hydrogen peroxide splitting on metal-free powders assisted by phosphoric acid as a stabilizer. *Nat. Commun.* **2020**, *11*, 3386.
(48) Iguchi, S.; Miseki, Y.; Sayama, K. Efficient Hypochlorous Acid (HClO) Production: Via Photoelectrochemical Solar Energy Conversion Using a $BiVO_4$-Based Photoanode. *Sustainable Energy Fuels* **2018**, *2*, 155−162.
(49) Okunaka, S.; Miseki, Y.; Sayama, K. Improvement of Photoelectrochemical HClO Production under Visible Light Irradiation by Loading Cobalt Oxide onto a $BiVO_4$ photoanode. *Catal. Sci. Technol.* **2021**, *11*, 5467−5471.
(50) *Guidelines for drinking-water quality: Fourth edition incorporating the first and second addenda*, World Health Organization (WHO), 2022 (https://www.who.int/publications/i/item/9789240045064).

https://doi.org/10.1021/jacsau.3c00066
JACS Au 2023, 3, 1403−1412

(51) Rice, E. W.; Clark, R. M.; Johnson, C. H. Chlorine inactivation of Escherichia coli O157:H7. *Emerg. Infect. Dis.* **1999**, *5*, 461−463.
(52) Horner, W. E.; Helbling, A.; Salvaggio, J. E.; Lehrer, S. B. Fungal Allergens. *Clin. Microbiol. Rev.* **1995**, *8*, 161−179.
(53) Tarr, H. L. A. Chemical disinfection and corrosion prevention. *J. Fish. Res. Board Can.* **1947**, *7*, 101−115.
(54) Zidouri, H. Desalination in Morocco and presentation of design and operation of the Laayoune seawater reverse osmosis plant. *Desalination* **2000**, *131*, 137−145.
(55) Yu, C. L.; Wei, L. F.; Chen, J. C.; Zhou, W. Q.; Fan, Q. Z.; Yu, J. Novel $AgCl/Ag_2CO_3$ heterostructured photocatalysts with enhanced photocatalytic performance. *Rare Met.* **2016**, *35*, 475−480.

https://doi.org/10.1021/jacsau.3c00066
JACS Au 2023, 3, 1403−1412